2010 IEEE International Conference on Robotics and Automation
Anchorage Convention District
May 3-8, 2010, Anchorage, Alaska, USA

Magnetic nanosheets manipulation: modeling, development and validation

V. Mattoli, *Member, IEEE*, E. Sinibaldi, V. Pensabene, *Member, IEEE*, S. Taccola, *Student Member, IEEE*, A. Menciassi, *Member, IEEE*, P. Dario, *Fellow, IEEE*

Abstract— **Polymeric ultra-thin films, also called nanosheets, show peculiar properties in terms of thickness, flexibility and chemical structure. For these reasons, they were proposed as nanoplasters for localized drug release or as a new solution for closing endoluminal surgical wounds. This paper presents the fabrication and characterization of free-standing nanosheets loaded with iron oxide nanoparticles, which can be manipulated in liquid environment by means of magnetic fields. A theoretical model of magnetic manipulation of the nanosheet is proposed and validated by dragging the film with a permanent magnet mounted on an industrial robotic arm. Controlling the magnetic sheet in liquid environment represents a first step towards the application of these nanostructures as free-standing carriers to be released and magnetically controlled in endoluminal surgery or as plasters with nanometric thickness to be delivered *in situ* on surgical incisions. Furthermore, these magnetic nanofilms can be adapted and used as micro and nanocomponents for the design of a novel generation of magnetic actuated polymeric microrobots.**

I. Introduction

NANOSHEETS are polymer-based films with very large area (up to tens of cm^2) and with a thickness in the order of few tens – hundreds of nanometers [1]. The peculiar properties of these structures make them suitable for different applications; in particular ultra-thin films have been developed for electrochemical devices, as chemical, biological and nano-mechanical sensors, and as nano-scale chemical and biological reactors [2]-[7]

The layer-by-layer fabrication process of polymers enables the fabrication of elastic films which can be modified, functionalized, cut and folded for building novel components of soft robots with micrometer size.

Biocompatibility, flexibility and possibility to carry drugs for controlled release are just some of the most interesting features that nanosheets can exploit [8]. They have been recently presented in the biomedical field for closing incisions after open surgery or laparoscopic procedures, using them as nanopatches or adding them to traditional sutures on wet tissues [9],[10]. For using nanosheets as plasters to be delivered, targeted and finely positioned *in situ* on surgical incisions, or to perform therapeutic or treatment tasks, nanosheets must be precisely manipulated. Thus, these nanostructures should be handled and positioned within a wet or liquid working environment, possibly by using non-invasive external tools [11]. Nowadays, the use of magnetic controlled systems is widely accepted and pursued, and several platforms are already employed, with computer-controlled permanent magnets and gradient coils, both at the clinical and the research level [12]-[14].

The possibility to include magnetic components into nanosheets, such as magnetic nanoparticles or nanobeads, represents a first step for the development of magnetic nanosheets with the potential of a remote controlled manipulation [15]. A target application could be the release of the nanosheet inside the body through a catheter in the context of NOTES [11],[16]. Anyhow, controlling and manipulating in a liquid environment ultra thin structures, homogeneously loaded with magnetic nanoparticles, is a complex problem requiring competence in magnetism and hydrodynamics. In this framework, we present first a theoretical section for modeling the interaction of a water suspended nanosheet under the control of an external magnetic field, and we derive the maximum dragging speed.

Towards the development of magnetic controlled nanosheets, we thus report in section III the fabrication and characterization of the polymeric nanostructure. A final experimental test bench is thus presented, including a controlled robotic arm for evaluating the effective *in liquid* magnetic manipulation of the nanosheets dragged by a specific permanent magnet. The fine control of nanosheet movement is beyond the scope of the present paper; it will be investigated in a subsequent work. Indeed, nanosheet manipulation under physiological conditions (e.g. within body organs) requires deeper understanding towards which the present study represent a first step.

Manuscript received September 15, 2009. This work was supported in part by the Italian Institute of Technology (IIT)

V. Mattoli is with IIT, Italian Institute of Technology, Genova, Italy (corresponding author phone: +39-050-883417; fax: +39-050-883497; e-mail: virgilio.mattoli@iit.it).

E. Sinibaldi (edoardo.sinibaldi@iit.it) is with IIT, Italian Institute of Technology, Genova, Italy.

V. Pensabene (virginia@crim.sssup.it) is with Scuola Superiore Sant'Anna, Pisa, Italy and she is also with IIT, Italian Institute of Technology, Genova, Italy.

S. Taccola is with Scuola Superiore Sant'Anna, Pisa, Italy (s.taccola@sssup.it)

A. Menciassi is with Scuola Superiore Sant'Anna, Pisa, Italy and she is also with IIT, Italian Institute of Technology, Genova, Italy (e-mail: arianna@sssup.it).

P. Dario is with Scuola Superiore Sant'Anna, Pisa, Italy, and he is also with IIT, Italian Institute of Technology, Genova, Italy (e-mail: dario@sssup.it).

II. NANOSHEET MAGNETIC MANIPULATION MODELING

In order to perform the control of a homogeneous magnetic nanosheet, a model for its interaction with an external magnetic field generated by a permanent cylindrical symmetric magnet moved by using an industrial robot is here proposed. Let us consider a hydrophobic magnetic nanofilm, buoyant at the free-surface between a liquid (water) and air. The steady-state nanofilm dragging movement due to an external moving magnet is then considered.

A. Magnet Model

The nanofilm is represented as a two-dimensional, squared patch having edge size l and embedding ferromagnetic nanoparticles (see Experimental section) which are distributed according to a density d_p.

Once introduced a Cartesian reference frame as sketched in Fig. 1, the external magnet is represented as a dipole having constant moment $\vec{M} = M\,\hat{e}_z$, placed at $\vec{P}_0 = (x_0, 0, h)$ and moving with (constant) velocity $v_0\,\hat{e}_x$. Let $\vec{P} = (x, y, 0)$ indicate a generic point on the patch; then, the magnetic field at $\vec{P}$, as produced by the dragging magnet, is given by [17]

$$\vec{B} = \frac{\mu_0}{4\pi}\left[\frac{3(\vec{M}\cdot\vec{r})\vec{r} - r^2\vec{M}}{r^5}\right] \qquad (1)$$

where μ_0 is the vacuum magnetic permeability, $\vec{r} = \vec{P} - \vec{P}_0$ and $r = \|\vec{r}\| = \left[(x - x_0)^2 + y^2 + h^2\right]^{1/2}$.

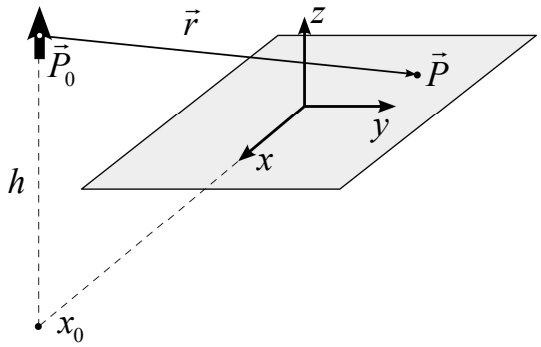

Fig. 1. Nanosheet and permanent magnet (approximated with a magnetic dipole) positioned in the Cartesian reference frame; the frame origin coincides with the nanosheet center.

B. Nanosheet Magnetic Interaction

The ferromagnetic nanoparticles embedded in the nanosheet are also modeled as magnetic dipoles. In particular, their dipole moment $\vec{m}_p$ is assumed to be proportional to the local magnetic field produced by the dragging magnet (in the considered magnetic field range): $\vec{m}_p = \chi_p\,\vec{B}$ where χ_p is a positive constant derived from the magnetic susceptibility of the nanoparticles [17]. Under this assumption, the generic particle undergoes a magnetic force $\vec{F}_p = \nabla(\vec{m}_p \cdot \vec{B}) = 2\,\chi_p\,\vec{B}\cdot\nabla\vec{B}$, resulting in a dragging action along the *x*-axis having the following expression:

$$F_{px} = 2\,\chi_p\left(B_x\frac{\partial B_x}{\partial x} + B_y\frac{\partial B_y}{\partial x} + B_z\frac{\partial B_z}{\partial x}\right) \qquad (2).$$

Once substituted the relevant expressions into (1) and after derivation, (2) can be recast as follows:

$$F_{px} = \alpha\,\frac{r^2 + 4h^2}{r^{10}}(x_0 - x) \qquad (3)$$

where $\alpha_p = 6\,\chi_p\left(\frac{\mu_0}{4\pi}M\right)^2$ is a constant.

It should be noticed that F_{px} does not depend on the sign of M (i.e. the same dragging is also obtained by inverting the external magnet poles), consistently with the aforementioned assumption regarding local induction on nanoparticles. In addition, F_{px} is an odd function with respect to $(x_0 - x)$, and therefore it is possible to only consider $x_0 \geq 0$ for studying its trend. The elementary dragging force on the patch surface element $dx\,dy$ is straightforwardly given by $dF_x = d_p\,F_{px}\,dx\,dy$. By further assuming the particle density d_p be a constant, the resulting patch dragging force finally reads:

$$F_x = d_p\,\alpha_p\int_{-l/2}^{l/2}dy\int_{-l/2}^{l/2}\frac{r^2 + 4h^2}{r^{10}}(x_0 - x)\,dx \qquad (4)$$

Once fixed the involved parameters $(x_0, h, d_p, \alpha_p, l)$, the expression (4) can be numerically integrated. A typical resulting trend of F_x versus x_0 is shown in Fig. 2. Such a curve is hereafter denoted by $F_x(x_0; h, d_p, \alpha_p, l)$. It should be noticed that F_x is null for $x_0 = 0$, by symmetry.

Furthermore, it monotonically decays towards zero for x_0 "large enough", by virtue of the power decay of the magnetic interaction with distance, while being positive and attaining a maximum in the intermediate range.

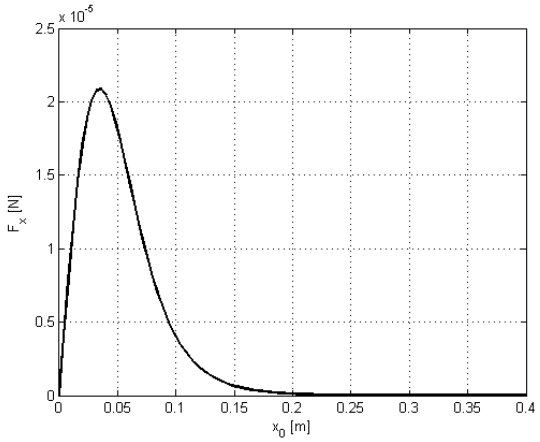

Fig. 2. Typical trend of $F_x(x_0; h, d_p, \alpha_p, l)$ as obtained by choosing $h = 10^{-1}$ m, $d_p = 2{,}27\ 10^{15}$ m^{-2}, $\alpha_p = 4{,}15\ 10^{-24}$ N m^7, $l = 1{,}5\ 10^{-2}$ m.

Let the maximum value of F_x be taken at $x_0 = \tilde{x}_0(h, d_p, \alpha_p, l)$, so that the corresponding dragging

force, once regarded to as a function of h, can be consistently denoted by $\widetilde{F}_x\left(h;d_p,\alpha_p,l\right)$. The considered trend of $\widetilde{F}_x$ versus h must be investigated numerically: a typical instance is shown in Fig. 3 for chosen values of the remaining parameters.

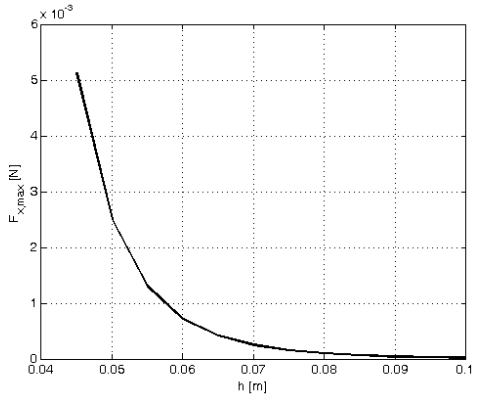

Fig. 3. Typical trend of $\widetilde{F}_x(h, d_p, \alpha_p, l)$ as obtained by choosing $d_p = 2{,}27\ 10^{15}$ m^{-2}, $\alpha_p = 4{,}15\ 10^{-24}$ N m^7, $l = 1{,}5\ 10^{-2}$ m.

It might be worth remarking that the x component of the magnetic force has been only considered for dragging. In fact we estimated that F_z do not affect the mono-dimensional model we propose.

C. *Freestanding nanosheet hydrodynamic interaction with liquid and dragging speed*

The aforementioned trend of $\widetilde{F}_x$ versus h can be directly exploited for obtaining the maximum allowed dragging speed $v_0^{\max}$ associated with the chosen parameter values, as explained below. To this purpose, we firstly consider the nanofilm as a purely two-dimensional flat plate having typical length l on which a fluid with density ρ and viscosity μ flows at speed v (this shear flow is assumed along a single side of the plate). At laminar regimes, the skin friction f_{fr} (force-per-length) acting on such a plate can be estimated by recalling classical fluid dynamics results [18], namely:

$$f_{fr} = \frac{1}{2}\rho v^2 l C_d\,, \qquad \text{where} \qquad C_d \cong \frac{2\zeta}{\sqrt{\mathrm{Re}_l}} \tag{5}$$

denotes the friction coefficient, depending on the Reynolds number $\mathrm{Re}_l = \rho v l / \mu$, and $\zeta = 0.664$ is a (non-dimensional) constant.

We then approximate the skin friction F_{fr} on a square plate by simply multiplying f_{fr} by l, thus neglecting boundary effects (more complex hydrodynamic modeling seems not to be fully justified in light of the present purposes). After substitution, the considered expression reads:

$$F_{fr} = \zeta\left(\rho\,\mu\right)^{1/2}\left(l\,v\right)^{3/2} \tag{6}.$$

Finally, an expression for the skin friction F_{sf} acting on the considered nanofilm is derived from (6), once replaced v with v_0 and by considering that both liquid (water) and air act on the nanofilm in this circumstance. However, air contribution is by far negligible with respect to the other (4 orders of magnitude), and therefore the sought expression can be approximated as follows:

$$F_{sf} \cong \zeta\left(\rho_w\,\mu_w\right)^{1/2}\left(l\,v_0\right)^{3/2} \tag{7}$$

where subscripts indicate water.

As a result, by equating $\widetilde{F}_x\left(h;d_p,\alpha_p,l\right)$ and F_{sf}, it is possible to obtain an estimation of the maximum dragging speed $v_0^{\max}$ as a function of the relevant parameters.

D. *Approximated Analytical Solution*

An analytical approximation can be introduced for $F_x\left(x_0;h,d_p,\alpha_p,l\right)$ when considering "small" patches. More rigorously, let $\lambda = \left[\,{x_0}^2 + h^2\,\right]^{1/2}$ be a characteristic length, to be used for defining the non-dimensional parameter $\varepsilon = l/\lambda$. By assuming $\varepsilon << 1$, it is possible to approximate (4) as follows:

$$F_x \cong d_p\,\alpha_p\,l^2\,\frac{\left(x_0^2 + 5\,h^2\right)x_0}{\left(x_0^2 + h^2\right)^5} \tag{8}$$

thus introducing an $o(\varepsilon^2)$ error. As shown in Fig. 4, this analytical approximation nicely matches the numerical solution as long as the working hypothesis $\varepsilon << 1$ is satisfied.

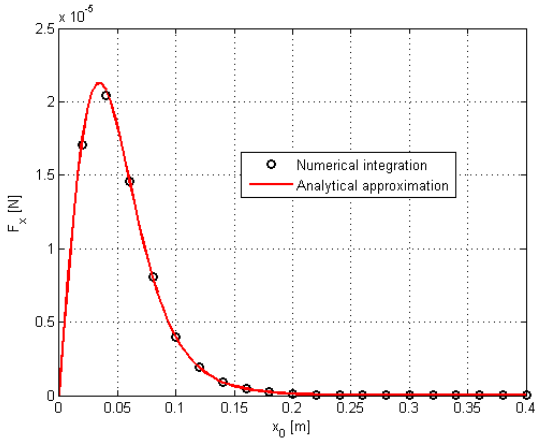

Fig. 4. Typical trend of $F_x(x_0; h, d_p, \alpha_p, l)$ as obtained by choosing $h = 10^{-1}$ m, $d_p = 2{,}27\ 10^{15}$ m^{-2}, $\alpha_p = 4{,}15\ 10^{-24}$ N m^7, $l = 1{,}5\ 10^{-2}$ m. In such a case, $\varepsilon \le l/h = 0{,}15$ and the analytical approximation (8) nicely fits the exact solution, obtained by numerical integration.

The value $\widetilde{x}_0$ at which the maximum dragging force occurs can be obtained by straightforward derivation of (8). In particular, an algebraic equation is obtained allowing for a single physically meaningful extremum at:

$$\widetilde{x}_0 \cong \xi\,h\,, \tag{9}$$

with $\xi = \sqrt{2\sqrt{17/7} - 3}$, the corresponding value being:

$$\widetilde{F}_x \cong d_p\,\alpha_p\,l^2\,\gamma\,h^{-7} \tag{10}$$

where $\gamma = \xi\left(\xi^2 + 5\right)/\left(\xi^2 + 1\right)^5$. It may be worth remarking once again that the expression (10) approximates the sought relation $\widetilde{F}_x\left(h;d_p,\alpha_p,l\right)$ under the working

hypothesis $\varepsilon << 1$ which, by virtue of (9), here becomes $l << \sqrt{1+\xi^2}\, h$. A corresponding typical trend is shown in Fig. 5.

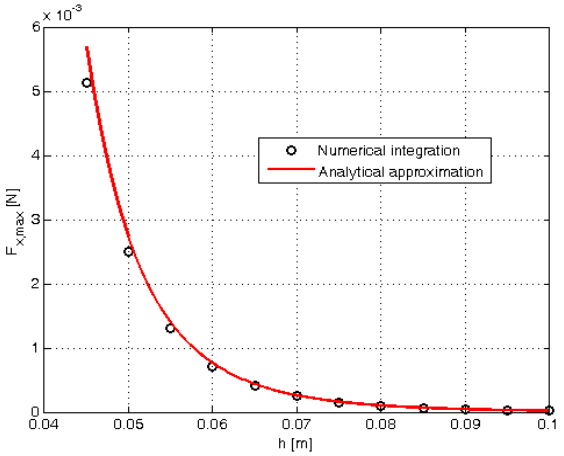

Fig. 5. Typical trend of $\widetilde{F}_x(h, d_p, \alpha_p, l)$ as obtained by choosing $d_p = 2{,}27\ 10^{15}$ m^{-2}, $\alpha_p = 4{,}15\ 10^{-24}$ N m^7, $l = 1{,}5\ 10^{-2}$ m. In such a case, $\varepsilon \le l/h = 0{,}3$ and the analytical approximation (10) nicely fits the exact solution, obtained by numerical integration.

Once $\widetilde{F}_x\left(h; d_p, \alpha_p, l\right)$ has been defined exploiting the analytical approximation in (10), it is also possible to estimate the corresponding maximum nanofilm dragging speed $v_0^{\max}$. When "small" patch approximation is applied, this estimation is readily provided by equating (7) and (10), thus obtaining:

$$v_{0\max} \cong \sigma\, l^{1/3}\, h^{-14/3} = k\, h^{-14/3} \tag{11}$$

with (by also recalling relevant definitions)

$$\sigma = \left(\frac{\gamma}{\zeta}\right)^{2/3} \left(\rho_w\, \mu_w\right)^{-1/3} \left(d_p\, \alpha_p\right)^{2/3} = \tag{12}$$

$$= \left(\frac{3\, \chi_p\, \gamma\, \mu_0^2}{8\, \zeta\, \pi^2}\right)^{2/3} \left(\rho_w\, \mu_w\right)^{-1/3} d_p^{2/3}\, M^{4/3}$$

$$k = \sigma\, l^{1/3}$$

III. Experimental

A. Nanosheet Fabrication

The magnetic free-standing nanosheet was fabricated by a single step spin-coating assisted deposition (sacrificial layer approach) [8]. It is composed by Poly L-lactic acid (PLLA) loaded with iron oxide (Fe_2O_3) nanoparticles (NPs) (200 nm of typical diameter).

The nanosheet film has been obtained by a sequential spinning of a Poly Vinyl Alcohol (PVA) solution (10 mg/ml in H_2O, for sacrificial layer) and PLLA dispersion of NPs (10 mg/ml NPs and 10 mg/ml PLLA in CH_2Cl_2).

Once defined the edges of the nanosheet with a cutter, the wafer was put in water which dissolves the sacrificial PVA layer thus obtaining a hydrophobic nanosheet free to float (free-standing nanosheets). More details on the fabrication procedures are available in [15].

Magnetic properties of used iron oxide nanoparticles have been previously characterized by superconducting quantum interference measurement device (SQUID) analysis (*SQUID magnetometer MPMSXL-7, Quantum Design).*

B. Drag experiments

In order to hold and move the magnetic nanofilm on the water surface, a permanent magnet has been mounted on a robotic arm. The robotic platform used in the study is a 6 degree of freedom (DoF) anthropomorphic robotic arm (RV-3SB, Mitsubishi Electric, Japan) and the permanent magnet (1.5 T axially magnetized neodymium cylindrical magnet, 50.8 mm of diameter and 25.4 cm of height) attached to the end-effector.

A set of dedicated experiments have been carried out to evaluate the maximum drag speed ($v_0^{\max}$) in different conditions. Experiments were conducted at different distance h (on z-axis, h ranging from 45 to 100 mm, with a resolution of 5 mm) between the magnet and the nanofilm center (the nanosheet was left free to float onto the surface of a water filled transparent container). Starting from a fixed initial position, with the magnet aligned along z-axis with the center of the nanofilm, the robotic arm was moved at a constant velocity v along the x-axis Fig. 6a. For each h distance, the procedure was repeated, gradually increasing the robotic arm velocity in step of 1 mm/s, up to reach the maximum drag speed ($v_0^{\max}$) over which the nanosheet stops to follow the movement of magnet.

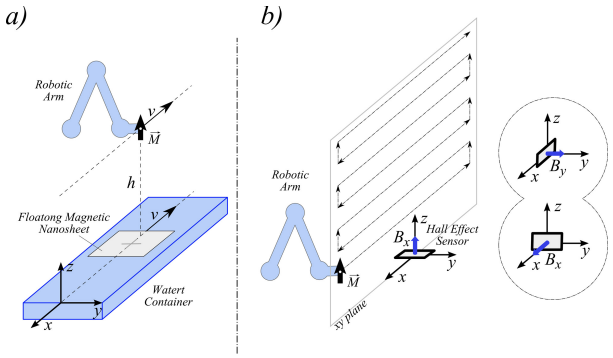

Fig. 6. a) Setup and reference frame for dragging experiments; repeated test are performed varying velocity v and distance h. b) Experimental setup and reference frame for magnetic field characterization;. the main scheme addresses the measurement of B_z component. Sensor configuration for B_x and B_y component measurements are reported on side.

C. Magnet Characterization Set-Up

To measure and characterize the magnetic field of the permanent magnet we used a Hall effect sensor (*SS94A2, Honeywell*) with a sensitivity of 5 mV/Gauss. Since the strength of a magnetic field varies with distance from the magnet, the Magnetic Field Sensor was fixed in a reference position (x=0, y=0 and z=0), while the magnet was moved by the robot along in the x-z plane, making several sweeping at constant speed (5 mm/s) along x-axis (ranging from -100 mm to 100 mm) at different value of z = h (h ranging

from 50 mm to 220 mm by 5 mm steps) (see Fig. 6a). The set of measurement has been repeated for each orientation of the sensor (along x, y and z axis), to measure the different component of the magnetic field (B_x, B_y B_z).

IV. Results and Discussion

A. Nanofilm Prototype

The obtained magnetic nanosheet has a surface of 15 x 15 mm^2 and an average thickness on the order of 200 nm (see Fig. 7). The microscopic morphology of nanosheets and distribution of the NPs inside the films have been deeply investigated [15]. By the morphological point of view, the nanosheet shows a relatively uniform NPs dispersion (see. Fig. 7). In general nanoparticles aggregates are quite small (tens of nanoparticles) and show an almost 2-D dimensional organization (thickness of film over the NPs aggregation measure is about 600-650 nm, independently on the aggregate extension, indicating a distribution of nanoparticles in a few layers).

The concentration of NPs in the nanofilm has been directly estimated from stoichiometric calculations. In particular the surface (mass) density of NPs results to be 5 10^{-2} kg/m^2, which can be expressed in term of numeral surface density as $d_p = 2{,}27\ 10^{15}\ m^{-2}$ (average NP volume of $4{,}19\ 10^{-21}\ m^3$ has been considered).

From SQUID measurement we obtained the value of NP bulk susceptibility $\chi = 6{,}4\ 10^2\ A^2\,m^3 / (N\,kg)$, from which is possible to calculate the susceptibility of a single (typical) NP: $\chi_p = 1{,}41\ 10^{-14}\ A^2\,m^3 / N$.

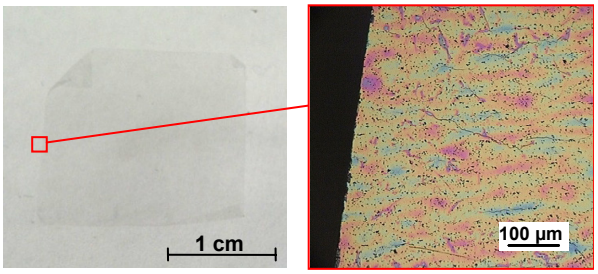

Fig. 7. An example of free-standing homogeneous magnetic nanosheet (20 x 20 mm^2) suspended in aqueous solution (left). On the right side, optical microscope picture shows the dispersion of magnetic NPs aggregates. For dragging experiments a smaller nanosheet (15x15 mm^2) has been used.

B. Magnet Characterization

From the characterization of the permanent magnet, carried out by means of the Hall effect sensor, it results that the generated magnetic field is consistent with dipole approximation, at least for a distance h > 50mm (in our experiments for h < 50mm the magnetic field saturates the sensor). In Fig. 8 and Fig. 9 we report respectively the field components B_x and B_z measured in function of the magnet position the x-z plane (sweep on x-axis at different *h* value on z-axis, with *h* measured from the center of magnet).

The behavior of experimental curves matches very well with the theoretical dipole field model, obtained by (1), that can be expressed in our frame as:

$$B_x = -3\,\frac{\mu_0}{4\pi} M \frac{x\,h}{r^5}\,; \tag{13}$$

$$B_z = M\,\frac{\mu_0}{4\pi}\,\frac{\left(3\,h^2 - r^2\right)}{r^5}\,. \tag{14}$$

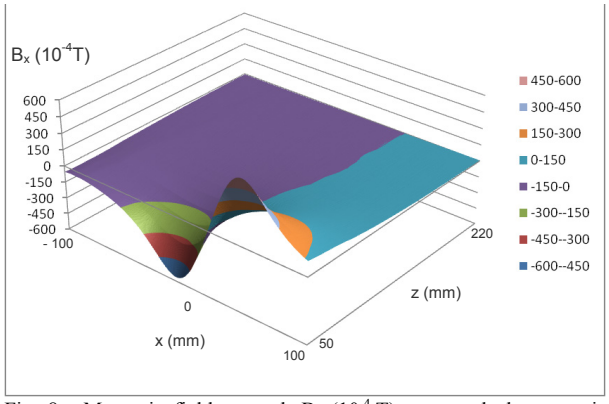

Fig. 8. Magnetic field strength B_x (10^{-4} T) measured along x-axis direction over xz plane; x position varies between -100 and 100 mm, z position between 50 and 220 mm.

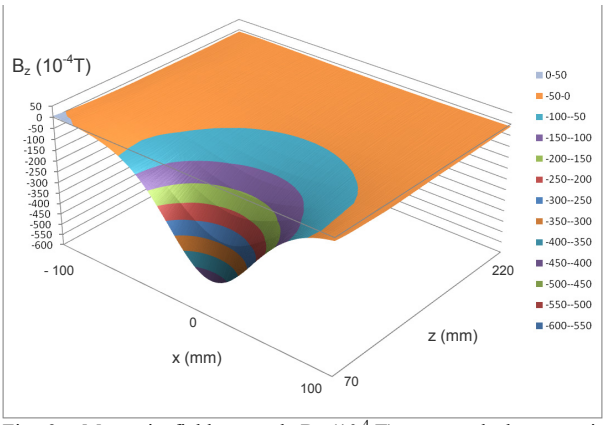

Fig. 9. Magnetic field strength B_z (10^{-4} T) measured along z-axis direction over xz plane; x position varies between -100 and 100 mm, z position between 70 and 220 mm.

It is noticeable that, being y = 0, B_y is almost null over the x-z plane (experimental results for B_y are congruent with theory, and for this reason they were omitted)

The obtained experimental results have been used to evaluate the magnetic moment *M* of the ideal magnet dipole equivalent to the permanent magnet.

From this estimation (made by fitting different subset of data), it results a magnetic moment M = 70 A m^2.

C. Drag Experiment Results and Model Validation

Drag tests have been carried out to find the relation between the maximum nanosheet dragging speed and the vertical distance of nanosheet from the magnetic dipole. From the theoretical model, it results a direct power correlation between this two parameters as expressed by equation (11). The obtained results are reported in graph in Fig. 10. The experimental points (red circles) (showing a very regular behavior) have been thus fitted with the function $k\,h^{-14/3}$ in order to find the best *k* value (named *k'*).

As it is possible to notice, the accordance of fitting curve with the experimental data is almost perfect, providing $\boldsymbol{k' = 1{,}17\ 10^{-6}\ m^{17/3}\ s^{-1}}$ as result.

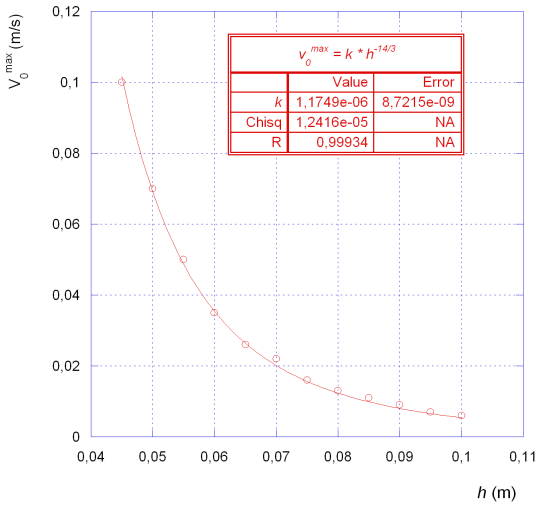

Fig. 10. Results of dragging tests: v_0^{max} vs h.: experimental points (red circles) and fitting curve (red line). From the fitting a value of $k' = 1{,}17\ 10^{-6}\ m^{17/3}\ s^{-1}$ was obtained.

To finalize the model validation, the found k' coefficient is thus compared with the value calculated from (12):

$$k = \left(\frac{3\,\chi_p\,\gamma\,\mu_0^2}{8\,\zeta\,\pi^2} \right)^{2/3} (\rho_w\,\mu_w)^{-1/3}\, d_p^{2/3}\, M^{4/3}\, l^{1/3}$$

Substituting all the constants and parameters in the equation, a $\boldsymbol{k = 1{,}50\ 10^{-6}\ m^{17/3}\ s^{-1}}$ is found. This value is in perfect agreement (not only as order of magnitude!) with the value obtained from the fitting.

V. Conclusions

The presented theoretical model is firstly based on the analysis of each component of the set up for the *in liquid* manipulation of the magnetic nanosheet, and then on the evaluation of the interaction between the magnetic source and the fabricated film. The magnetic field generated by the permanent magnet is described in this model as a dipole, and the measurements obtained by Hall Effect sensor in the surrounding 2D space are perfectly consistent. The theoretical model of the hydrophobic magnetic nanofilm, which flows at the free-surface between a liquid (with fixed density ρ and viscosity μ) and air, returns the expression of the maximum magnetic drag force, which is also proportional to $h^{-14/3}$. This is in complete accordance with the experimental evidence, with a slight difference between the nominal and effective constant k value. The study of the magnetic manipulation of the nanosheet thus provides a initial precise model, while the organized experimental test bench represents a useful platform for evaluating the potential use of polymeric magnetic nanofilms in liquid environment, in particular concerning control and position

Acknowledgment

The authors would like to thank the Italian Ministry of Foreign Affairs, General Directorate for Cultural Promotion and Cooperation for its support to the RoboCasa Laboratory in Tokyo and for funding the collaboration between the authors and the group of Prof. Takeoka at the Dept. Life Sci. Med. Biosci. of the Waseda University in Tokyo. In addition, they wish to thank Mr Gastone Ciuti for his technical and scientific support in carrying on the experimental test with the robotic platform.

References

[1] T. Fujie, Y. Okamura, S. Takeoka, "Ubiquitous Transference of a Free-Standing Polysaccharide Nanosheet with the Development of a Nano-Adhesive Plaster". *Adv Mater*, vol. 19, pp. 3549–3553, 2007.

[2] Y. Lvov, K. Ariga, I. Ichinose, T. Kunitake, "Assembly of multicomponent protein films by means of electrostatic layer-by-layer adsorption", *J. Am. Chem. Soc*., vol. 117, pp. 6117–6123, 1995..

[3] G. Decher, Y. Lvov, J. Schmitt, "Proof of multilayer structural organization in selfassembled polycation-polyanion molecular films", *Thin Solid Films*, vol. 244, pp. 772–777, 1994.

[4] V.V. Tsukruk, V.N. Bliznyuk, D. Visser, A.L. Campbell, T.J. Buning, W.W. Adams, "Electrostatic deposition of polyionic monolayers on charged surfaces", *Macromolecules*, vol 30, pp. 6615–6625, 1997.

[5] L. Zhai, F.C. Cobeci, R.E. Cohen, M.F. Rubner, "Stable superhydrophobic coatings from polyelectrolyte multilayers", *Nano Lett.*, vol. 4, pp. 1349–1353, 2004.

[6] C. Jiang, V.V. Tsukruk, "Freestanding nanostructures via layer-by-layer assembly", *Adv. Mater*, vol. 18, pp. 829–840, 2006.

[7] Z. Tang, Y. Wang, P. Podsiadlo, N.A. Kotov, "Biomedical applications of layer-by-layer assembly: from biomimetics to tissue engineering", *Adv. Mater.*, vol. 18, pp. 3203–3224, 2006.

[8] Y. Okamura et al. "Fabrication of free-standing nanoparticle-fused nanosheets and their hetero-modification using sacrificial films", *Colloids and Surfaces A*, vol. 318, pp. 184–190, 2008.

[9] Y. Okamura, K. Kabata, M. Kinoshita, D. Saitoh, and S. Takeoka, "Free-Standing Biodegradable Poly(lactic acid Nanosheet for Sealing Operations in Surgery", *Adv. Mater*., vol. 21, pp. 1–5, 2009..

[10] T. Fujie, N. Matsutani, M. Kinoshita, Y. Okamura, A. Saito, S. Takeoka, "Adhesive, Flexible, and Robust Polysaccharide Nanosheets Integrated for Tissue-Defect Repair", *Adv. Funct. Mater*, vol. 19, pp. 1–9, 2009.

[11] V. Pensabene, V. Mattoli, T. Fujie, A. Menciassi, S. Takeoka, P. Dario "Magnetic nanosheet adhesion to mucosal tissue", in *Proc. IEEE Nano*, Genova, 2009, pp. 489-493

[12] Available: http://eu.stereotaxis.com/Products-Technology/Magnetic-Navigation/

[13] S. R. Atmakuri, E. I. Lev, C. Alviar, E. Ibarra, A. E. Raizner, S. L. Solomon, N. S. Kleiman, "Initial Experience With a Magnetic Navigation System for Percutaneous Coronary Intervention in Complex Coronary Artery Lesions", *Journal of the American College of Cardiology*, Vol. 47, no.3, pp. 515-521, 2006

[14] S. Martel, J.B. Mathieu, O. Felfoul, A. Chanu, E. Aboussouan, S. Tamaz, and P. Pouponneau. "Automatic navigation of an untethered device in the artery of a living animal using a conventional clinical magnetic resonance imaging system". *App. Phys. Lett.*, vol. 90, 2007.

[15] V. Mattoli, V. Pensabene, T. Fujie, S. Taccola, A. Menciassi, S. Takeoka, P. Dario, "Fabrication and characterization of ultra-thin magnetic films for biomedical applications", in *Proc. Eurosensors XXIII*, Lausanne, 2009, pp. 28-31

[16] E. Sinibaldi, V. Pensabene, S. Taccola, S. Palagi, A. Menciassi, P. Dario, V.Mattoli, "Magnetic nanofilm for biomedical applications"in *Proc.* of Global Congress on NanoEngineering for Medicine and Biology *NEMB2010*, Houston, TX, USA, February 7-10, 2010.

[17] Halliday, Resnick, Fundamental of Physics, Wiley & Sons Ltd., 2007

[18] F. M. White, Viscous fluid flow, McGraw-Hill, 2005